CHAPTER 63

EFFECTS OF BLAST LOADING ON A PIER

Young C. Kim
Associate Professor of Civil Engineering
California State College at Los Angeles
Los Angeles, California, U.S.A.

Thorbjorn Karlsson
Senior Research Engineer, Science Engineering Associates
San Marino, California, U.S.A.

William L. Ko
Senior Research Engineer, Southwest Research Institute
San Antonio, Texas, U.S.A.

ABSTRACT

The effects of nuclear explosions on a pier have been investigated to study the interaction phenomena between the blast loading, induced surface waves, the beach geometry, and the depth of coastal region for purpose of damage assessment and protective design of a coastal structure.

For the theoretical analysis, the diffraction pattern predicted by Whitham's theory was used. The characteristic solution for shock diffraction showed the shock front shapes, shock-shock shapes, and flow rays in the pier and beach geometry. A pier model was tested in a six foot diameter horizontal shock tube under four different test situations simulating pier on a beach with water, pier on a dry beach in a Mach reflection region, pier in deep water, and a pier on a dry beach in a region of regular reflection. The model was subjected to various shock overpressures in each of the four test situations.

Transient pressure distribution on the pier was investigated and comparison between the characteristic solution and the test results was made.

INTRODUCTION

The study of loads encountered by coastal structures, such as piers and docks, has in the past been concerned mainly with the action of waves on such structures. There are, however, other types of loads, which may be of concern in certain locations and their effects upon these structures need to be investigated. Among those are loads caused by air blasts and explosions. It is entirely conceivable that uplift forces on a pier deck caused by trapped air underneath or by blast induced water waves can cause heavy damage on those structures.

This paper describes an experimental program which was undertaken in order to obtain a better understanding of the effects of air blast on a pier. An objective of the investigation was to compare the test results with those predicted by existing theories and to make recommendations pertaining to the use of the experimental results for design and damage assessment.

The experiments were conducted in a six foot diameter shock tube in which a metal pier model was mounted. The paper describes the experimental investigation and presents the test results. These results are compared with theoretical results obtained graphically by the method of characteristics based upon Whitham's theory of shock-shock diffraction.

THEORY OF DIFFRACTION OF A STRONG SHOCK BY AN OBSTACLE

When a strong shock wave impinges on an obstacle it is reflected. Since the reflected shock wave always travels through air which has been heated and compressed by the passage of the incident wave, it travels faster than the incident shock wave and may eventually overtake the incident shock wave front. As a result, the two waves are fused together and form a simple front, the so-called "Mach stem" (or Mach shock) (Ref. 1). Such a reflection is therefore called the Mach reflection in contrast to the regular reflection where the two shocks do not merge. The gas swept up by the Mach stem will flow alongside gas which has passed through both the incident and reflected shocks. Thus a contact discontinuity should pass through the so-called "triple point" where the incident front, the reflected front and the Mach stem intersect.

Whitham's Theory (Refs. 2 to 7) predicts the shape and location of the diffracted shock (Mach shock) at any time. The theory does not predict the shape or location of reflected shocks. As part of the description of the Mach shock the locus of successive positions of the Mach triple point can be found. Whitham calls this locus a "shock-shock," since it represents a Mach shock moving along the incident shock. The basic equations given by Whitham (Refs. 3, 8) for Mach diffractions are

1. Relationship between the ray area A and the Mach number M

$$A = k\, f(M) \tag{1}$$

where

k is an arbitrary constant
f(M) is given by

$$\begin{aligned} f(M) = \exp \{ -[& \log \frac{M^2-1}{M} + \frac{1}{\gamma} \log \left(M^2 - \frac{\gamma-1}{2\gamma}\right) + \log \frac{1-\mu}{1+\mu} \\ & + \left(\frac{\gamma-1}{2\gamma}\right)^{\frac{1}{2}} \log \left(\mu + \left(\frac{2\gamma}{\gamma-1}\right)^{\frac{1}{2}}\right) - \left(\frac{\gamma-1}{2\gamma}\right)^{\frac{1}{2}} \log \left(\mu - \left(\frac{2\gamma}{\gamma-1}\right)^{\frac{1}{2}}\right) \\ & + \left(\frac{2}{\gamma(\gamma-1)}\right)^{\frac{1}{2}} \log \left(\left(M^2 + \frac{2}{\gamma-1}\right)^{\frac{1}{2}} + \left(M^2 - \frac{\gamma-1}{2\gamma}\right)^{\frac{1}{2}}\right) \\ & + \left(\frac{1}{2(\gamma-1)}\right)^{\frac{1}{2}} \tan^{-1} \left(\frac{(4\gamma - (\gamma-1)^2)M^2 - 4(\gamma-1)}{4\gamma^{\frac{1}{2}}(\gamma-1)(M^2+2/(\gamma-1))^{\frac{1}{2}}(M^2-(\gamma-1)/2\gamma)^{\frac{1}{2}}}\right)] \} \end{aligned} \tag{2}$$

where

$$\mu^2 = \frac{(\gamma-1)M^2 + 2}{2\gamma M^2 - (\gamma-1)} \tag{3}$$

and γ is the ratio of specific heats for the gas.

2. Relationship between the characteristic angle m and the Mach number M

$$m = \tan^{-1} \left[\frac{(M^2-1)K(M)}{2M^2}\right] \tag{4}$$

where

$$K(M) = 2 \left[\left(1 + \frac{2}{\gamma+1}\,\frac{1-\mu^2}{\mu}\right)\left(2\mu + 1 + \frac{1}{M^2}\right)\right]^{-1} \tag{5}$$

3. The integral ω corresponding to the Prandtl-Meyer function in supersonic flow is given by

$$\omega = \int_1^M \left[\frac{2}{(M^2-1)\;K(M)}\right]^{\frac{1}{2}} dM \tag{6}$$

Therefore for two-dimensional Mach diffraction the characteristics of Whitham's diffraction equations (Ref. 3) are given by

$$\theta \pm \omega = \text{constant} \tag{7}$$

along curves of slope

$$\frac{dy}{dx} = \tan\,(\theta \pm m) \tag{8}$$

4. The shock-shock jump conditions for oblique shock-shock are given by

$$\tan(\chi-\theta_o) = \frac{A_o}{M_o}\left(\frac{M_1^2-M_o^2}{A_o^2-A_1^2}\right)^{\frac{1}{2}} \tag{9}$$

and

$$\tan\,(\theta_1-\theta_o) = \frac{(M_1^2 - M_o^2)^{\frac{1}{2}}\,(A_o^2 - A_1^2)^{\frac{1}{2}}}{A_1M_1 + A_oM_o} \tag{10}$$

where the subscript o refers to the flow before, the subscript 1 to the flow behind the shock-shock, θ_1 is the angle between the ray direction and the x-axis (see Fig. 1), and χ is the angle between the shock-shock and x-axis.

Figs. 2a, b show the full characteristic field, the constructed shock front shapes, shock-shock shapes, and flow rays in the test section of the shock tube for a dry beach. Peak overpressures of 23.3 psi and of 70 psi were chosen for analysis. The procedure for constructing Fig. 2a is described briefly below.

For the case of Fig. 2a the Mach number of the undisturbed shock is $M_o = 1.65$ and the corresponding characteristic angle and the Prandtl-Meyer integral, respectively, are $m_o = 20.295^o$, $\omega_o = 2.249$ rad. (Ref. 8). The characteristic corresponding to $m_o = 20.295$ deg. is labeled by 0 - 0. At

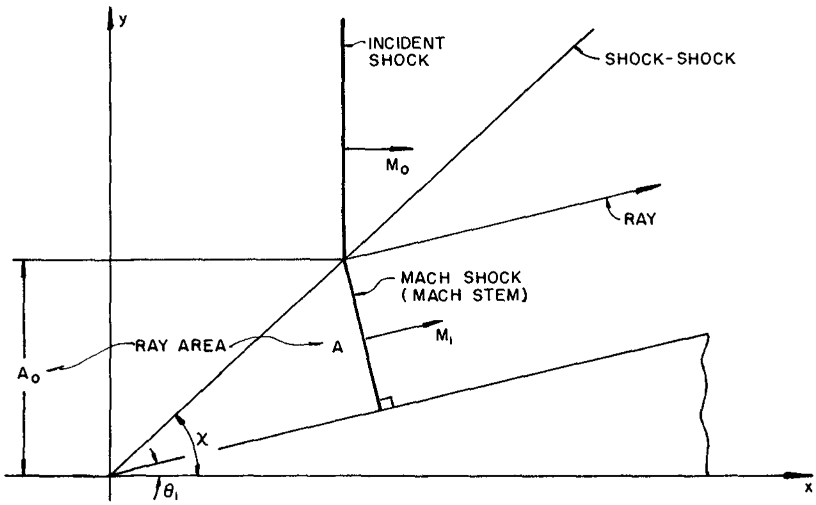

FIGURE 1 MACH DIFFRACTION BY A WEDGE

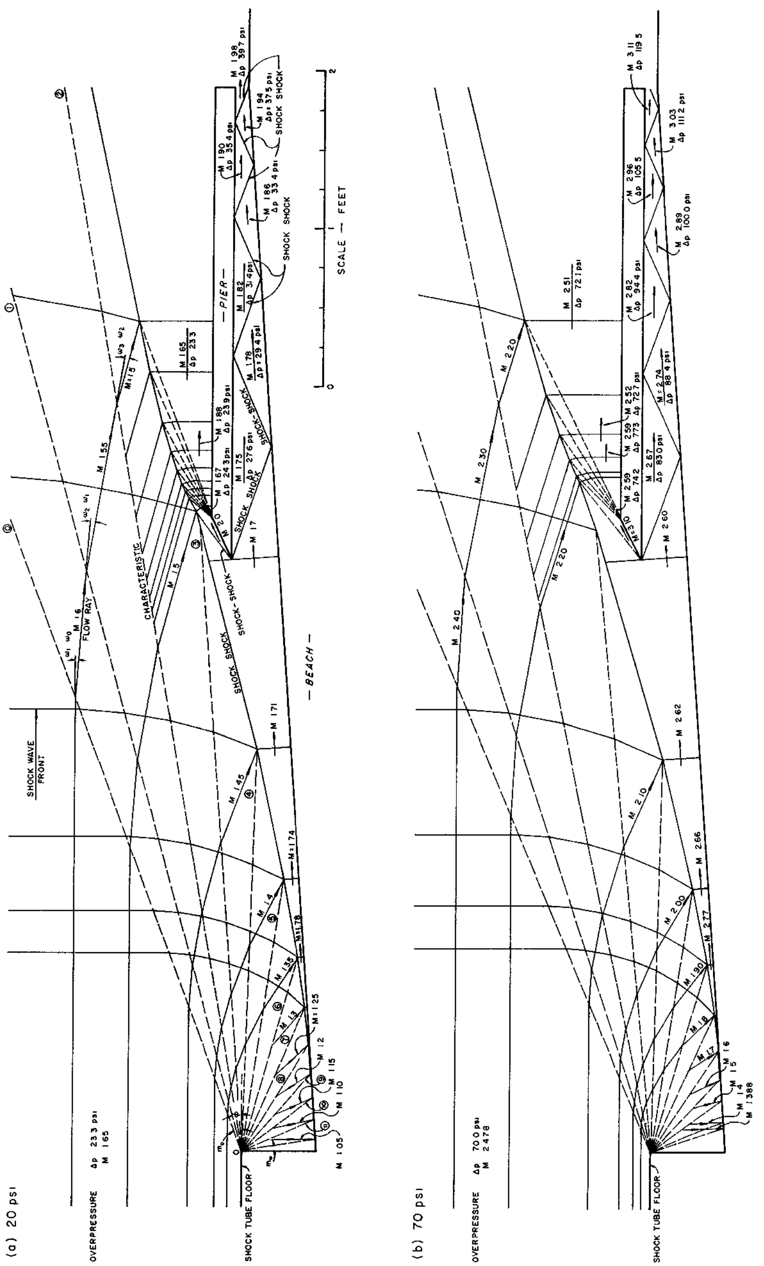

FIGURE 2 CHARACTERISTIC SOLUTION FOR SHOCK DIFFRACTIONS (BEACH SLOPE 1:14.25)

the convex corner θ_1 jumps from zero to negative 90^o and the solution is a centered simple wave. Neglecting reflection of the characteristics from the shock-shock, the characteristics are straight lines along which all flow properties are constant. After 90^o expansion the Prandtl-Meyer integral is given by

$$\omega_w = \omega_\sigma - \pi/2 = 2.249 - 1.57 = 0.679 \text{ radians}$$

where Eq. (7) is used. The Mach number and characteristic angle corresponding to this number are found to be

$$M_w = 1.059$$

$$m_w = 9.056^o$$

where the subscript w signifies flow along the vertical wall. Between M_o = 1.65 and M_w = 1.059, one may choose a series of different Mach numbers (eleven for the present example) and draw the characteristic fans as shown in Fig. 2. The flow field can be made as smooth as desired by increasing the number of characteristics running out from point O. The inclination of each characteristic line with respect to the horizontal line is calculated as follows. Consider the characteristic 0 - 1 corresponding to M - 1.6. One finds $m_1 = 19.983^o$, ω_1 = 2.165 rad. The angle of inclination ϕ_1 is then

$$\phi_1 = m_1 + (\omega_1 - \omega_o) \times 57.4^o = 15.163^o$$

and the angle of deflection of flow ray is

$$(\omega_o - \omega_1) \times 57.4^o = 4.82^o$$

This process is repeated for all Mach numbers.

When a flow ray is deflected by the beach wall Mach reflection takes place. The angles of flow deflection at point 11 (M = 1.1) and 10 (M = 1.15) are greater than 70^o and the shock-shock is found to be attached to the wall. At point 9 (M = 1.2) the flow deflection angle is $\theta_1 = 60^o$ and the shock-shock angle is found to be $\chi - \theta_1 \approx 0.2^o$ and the shock-shock between points 10 and 9 can be drawn. This process is repeated for constructing the entire shock-shock. When the Mach stem impinges on the pier a secondary shock-shock is formed The Mach number for any location of the Mach stem can be easily obtained for a given angle of deflection and an incident Mach number. Overpressure at a point is obtained from the pressure jump condition

$$\frac{\Delta p}{p_a} = \frac{p-p_a}{p_a} = \frac{2\gamma}{\gamma+1} (M^2 - 1) \qquad (11)$$

where p_a is the ambient pressure ahead of the shock front, p is pressure behind the shock front traveling at Mach number M based on the speed of sound ahead of the shock front, and γ is the ratio of specific heats of the gas. It is seen from Fig. 2 that due to the continuous deflection of the flow ray, the pressure on the lower side of the pier increases in the direction of flow.

It is to be kept in mind that the above characteristic solution is based on the following assumptions:

1. The flow is two-dimensional.
2. The incident shock front is plane.
3. Pier legs and obstacles on the pier surfaces are neglected.
4. Reflection of the characteristics from the shock-shock is neglected.

EXPERIMENTAL INVESTIGATION

The model tests were conducted in a six foot horizontal shock tube at the E. H. Wang Civil Engineering Research Facility (WCERF) of the University of New Mexico and the U. S. Air Force Weapons Laboratory at Albuquerque, New Mexico. The tube is made of steel, 6 feet in diameter and 246 feet long with one end closed. It is made up of 21 sections varying in length from 5 to 20 feet with heavy flanges at either end, which permit the various sections to be bolted together. The tube has a constant circular cross section for a distance of 144 feet downstream from the compression chamber door (closed end) at which point it changes to a partially circular cross section for the remaining length of the tube. The far end of the tube is left open. The blast wave in the shock tube is generated by the detonation of primacord which can produce overpressure ranging from 0 to 100 psi. The primacord consists of a flexible plastic tubing with a PETN (pentaery-thritoltetranit-rate, $C_5H_8(NO_3)_4$) core wrapped in a cotton cloth.

The model pier deck was 36.0" long by 6" wide by 1.5" thick and was made up of two steel plates, 3/4" thick each. The deck was supported by six cylindrical steel legs, 1" OD x 36" long. A steel plate (6'9" x 3'9" x 7/16") was located underneath the pier model with a slope of 1 to 14.25 to simulate a beach in a coastal region. The beach could be removed leaving the underside of the pier 13-1/2" above a level bottom to simulate deep water conditions. The pier model was located in a specially designed closure device on an adjustable base at a point approximately 180 feet from the blast. The closure device was rolled under the test section and raised into place to close the tube opening.

Pressure measurements in the shock tube and on the pier model were made with piezoelectric type transducers. The piezoelectric transducer essentially converts a pressure variation into a corresponding electric charge variation. The relationship is linear over a limited pressure and temperature range. The tranducers used were of the "ST" gage series manufactured by the Susquehanna Instrument Company. This gage series utilizes lead zirconate sensing elements. The model used was the ST-2 (1/2" diameter housing x 5/8" long) which is used primarily for pressure measurements of shock waves in air since it is capable of measuring fast-rise phenomena without ringing. This gage has a charge sensitivity of 20 picocoulombs per psi, a natural frequency of 250 kc, and a rise time of the order of 5-10 μ sec. A total of eleven ST-2 gages were used. Four of those were placed in the test section in the vicinity of the pier model for measuring the free field pressure. The pier model was instrumented with seven pressure gages with three facing upward and four facing downward. In addition to the above gages, one strain gage type transducer, the Schaevitz-Bytrex Model No. HFG-2000, was used in the free field.

Each day before starting tests every transducer was calibrated individually for output, pulse response characteristics, and linearity according to the procedure described in Ref. 9. A check on the pressure measurements was obtained by measuring the velocity of the shock wave as it passed through the test section. The shock velocity, U, is easily found since the distances between the gages are known. The shock overpressure is evaluated by using the one-dimensional relationship between pressure and Mach number

$$\frac{\Delta p}{p_a} = \frac{p - p_a}{p_a} = \frac{2\gamma}{\gamma+1}(M^2-1)$$

where p_a is the ambient pressure, γ is the ratio of specific heats for air, and M is the Mach number. The pressure-time variations measured by the various gages during the tests were recorded on magnetic tape as well as photographed from oscilloscope screens. The data recording equipment in use at the WCERF is described in Ref 9.

The pier model was tested in the following four situations:

(a) Pier located above a beach with a slope of 1 to 14.25 and with clearance of 1" between the underside of the shore end of the pier deck and still water level. This situation was intended to represent a pier in shallow water on a sloping beach (Fig. 3a).

(b) Pier located as in (a) but without water. This situation represents a pier on a dry beach in a Mach-reflection region (Fig.3b).

(c) The beach was removed so that the underside of the pier was located 13-1/2" above a level bottom and 1" above the still water surface. This situation represents a pier or platform in deep water (Fig. 3c).

(d) Pier located above beach with 1 to 14.25 slope without water and with clearance of 1" between the underside of the shore end of the pier deck and the beach as shown in Fig. 3d. This situation was intended to represent a pier on a dry beach in a regular reflection region.

In each of the four different situations, the pier model was subjected to five different shock overpressures. The five different overpressures and other shock characteristics were intended to be as follows:

Test No.	Peak Overpressure psi	Duration of Positive Pulse msec	Shock Velocity fps
1	5	70	1400
2	10	85	1500
3	20	100	1700
4	40	120	2100
5	70	135	2700

Three test runs were made at each pressure level. A total of 3 x 4 x 5 = 60

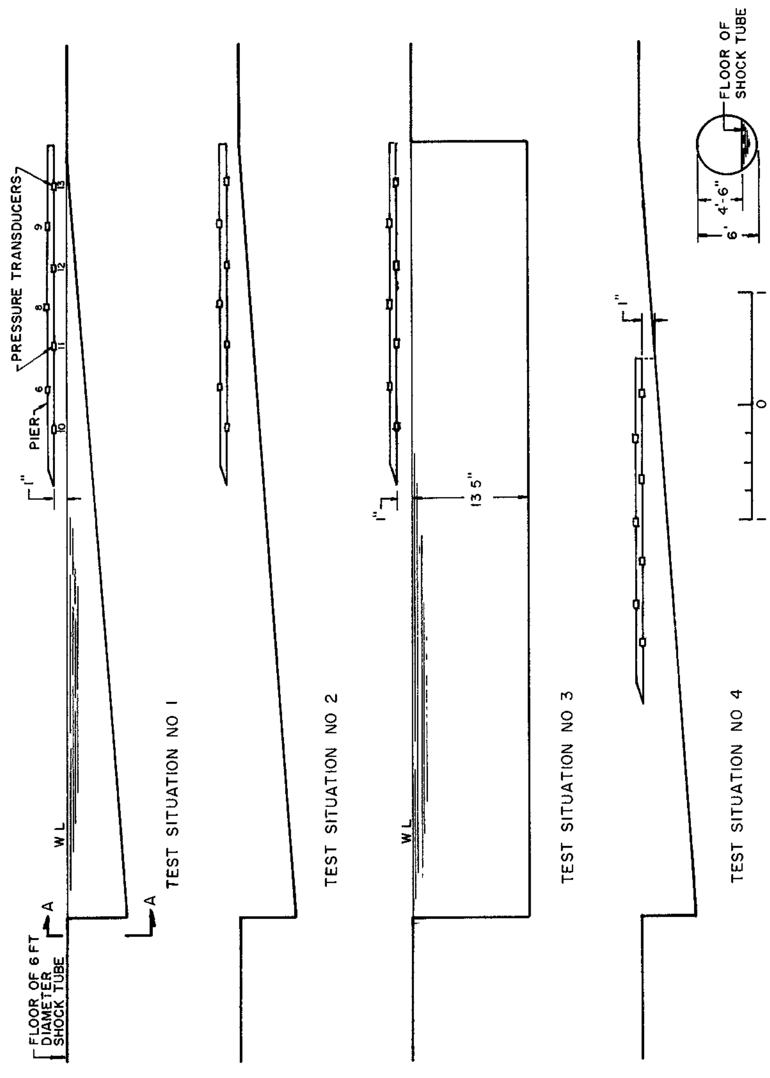

FIGURE 3 TEST SITUATIONS (BEACH SLOPE 1:14.25)

test runs were therefore performed.

ANALYSIS AND DISCUSSION OF RESULTS

The test results were obtained both in the form of magnetic tape recordings and photographic pressure-time diagrams. The photographic records were used to obtain the peak overpressure, impulse strength, and pulse duration at each gage location. In order to obtain a better basis for comparison between the various test situations these values have been normalized to the corresponding free field overpressure. In most instances the means are obtained from two out of the three runs, using the two in closest agreement. In a few cases the three runs gave almost identical values and were therefore all used to obtain the means. In one case (situation 2, 5 psi) only one run was used, since it was the only one close to the desired pressure level.

The reason for normalizing the peak overpressures may need some clarification. Each of the four test situations is tested at five different incident pressure levels. For obvious reasons, however, the intended pressure level is never obtained exactly. For example, the mean free field overpressure levels for the 20 psi overpressure runs were as follows:

Test situation no.	1	2	3	4
Mean free field overpressure, psi	21.1	19.3	20.4	20.5

It is clear that a meaningful comparison between the different test situations is not obtained directly from the pressure readings. While the pressure at any point on the pier is not likely to be a linear function of the free field pressure it seems reasonable to assume that in a narrow region of free field pressure the variation can be approximated by a straight line. On this basis all pressure readings have been normalized to the corresponding free field pressure and the result treated as the normalized pressure for the corresponding nominal pressure level.

A peculiarity is observed in the records from the lowest pressure tests, i.e., where the shock overpressure was less than 5 psi. The records show a double peaked pressure-time relationship at all channels. These two peaks are present in the intended 5 psi tests for test situations 1, 3, and 4, where the peak overpressure is around 3 psi. The very first run of test situation 2, where the shock overpressure is of the order of 2 psi, also shows double pressure peak at all channels. In subsequent runs of test situation 2 when the overpressure is 6-7 psi and higher, the second peak is no longer present. This is also the case for all other test situations until the highest pressure levels of 40-70 psi are reached. At those pressures multiple peaks are observed for test situations 1 and 3 (i.e., with water) at some of the gages located on the pier, whereas all the free field gages show a single peak. The double peak phenomenon at low pressure levels is probably caused by the reflected shock wave from the closed compression chamber end. The reflected shock, moving through air heated and compressed by the direct wave, travels faster than the direct wave and will eventually overtake it. At very low pressures the difference between the two wave speeds is small so that the reflected wave has not yet caught up with the direct wave as it reaches the test section, resulting in the double-peaked pressure-time record.

As noted above, the multiple pressure peaks at the highest pressure levels are observed only in test situations 1 and 3, i.e., where water is present. The first peak observed is most likely caused by the shock wave whereas subsequent peaks are seemingly due to water splashing on the pier model. These effects, however, could not be observed, since the test section of the shock tube was completely closed. It would be desirable in future tests to use high speed photography to find out what happens in the test section.

The values of normalized net peak pressures on the pier for 40 psi normal overpressure are shown graphically on Fig. 4. This is found as the difference between top and bottom pressures, assuming linear variation between gages. These represent essentially the peak loading on the pier model caused by the blast. The shock wave travels at a speed ranging from 1300 to 2800 fps which means that its travel time over the length of the pier model ranges from 2.3 to 1.1 milliseconds. The pulse duration on the pier is found to vary between 40-120 milliseconds. Thus the travel time of the wave over the length of the pier model is at most approximately 5% of the pulse duration indicating that no appreciable reduction in pressure has taken place at the front end of the pier when the wave arrives at the back end. The effect of water splashing on the pier which was discussed above is not included in Fig. 4. Since the relative wave arrival time at the various gages was not recorded, there is no way to assess the net pressure on the pier caused by the water impact. It should be kept in mind, however, that this effect could conceivably result in much higher uplift pressures than observed during the passage of the shock wave front.

The general trend for all test situations seems to be that the relative net uplift pressure increases very rapidly as the free field pressure is increased, especially at the front end of the pier. However, it is rather difficult to determine any definite trends for the different test situations. A better view is offered in Figs. 5-8 where the normalized pier pressures at each gage have been plotted against the free field pressure. Figs. 5-8, showing the peak pressure at the gages located on the top of the pier, reveal a similar behavior of each gage for all four test situations indicating that these peak pressures are not appreciably affected by the configuration in front of and underneath the pier, with the possible exception of situation #2 (Fig. 6a). This is really not surprising since these are pressures at the shock wave front and any effects of the bottom configuration are not likely to be felt until somewhat later. Fig. 6a shows the effects of the Mach reflection (Fig. 2), resulting in lower peak pressures on the pier top.

Figs. 5b - 8b, showing the peak pressures at the gages located on the underside of the pier, indicate a marked difference between the various test situations. Fig. 6b, showing the situation for a pier on a dry beach, indicates a very sharp relative pressure rise as the free field shock pressure increases, especially at the front end of the pier. The presence of water tends to reduce this pressure appreciably as Fig. 5b shows. Fig. 7b shows the results for a pier in deep water. When compared with Fig. 5b (pier on a beach with water) the difference between the two is negligible at low

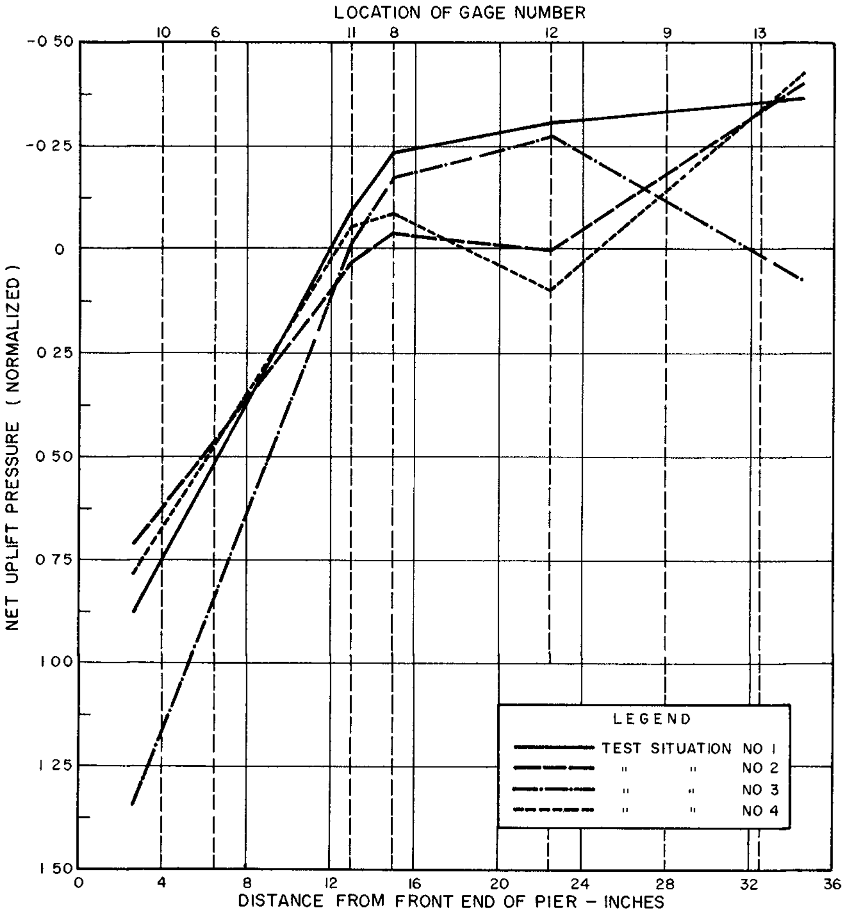

FIGURE 4 DISTRIBUTION OF NORMALIZED PEAK UPLIFT PRESSURE - 40 PSI NOMINAL OVERPRESSURE

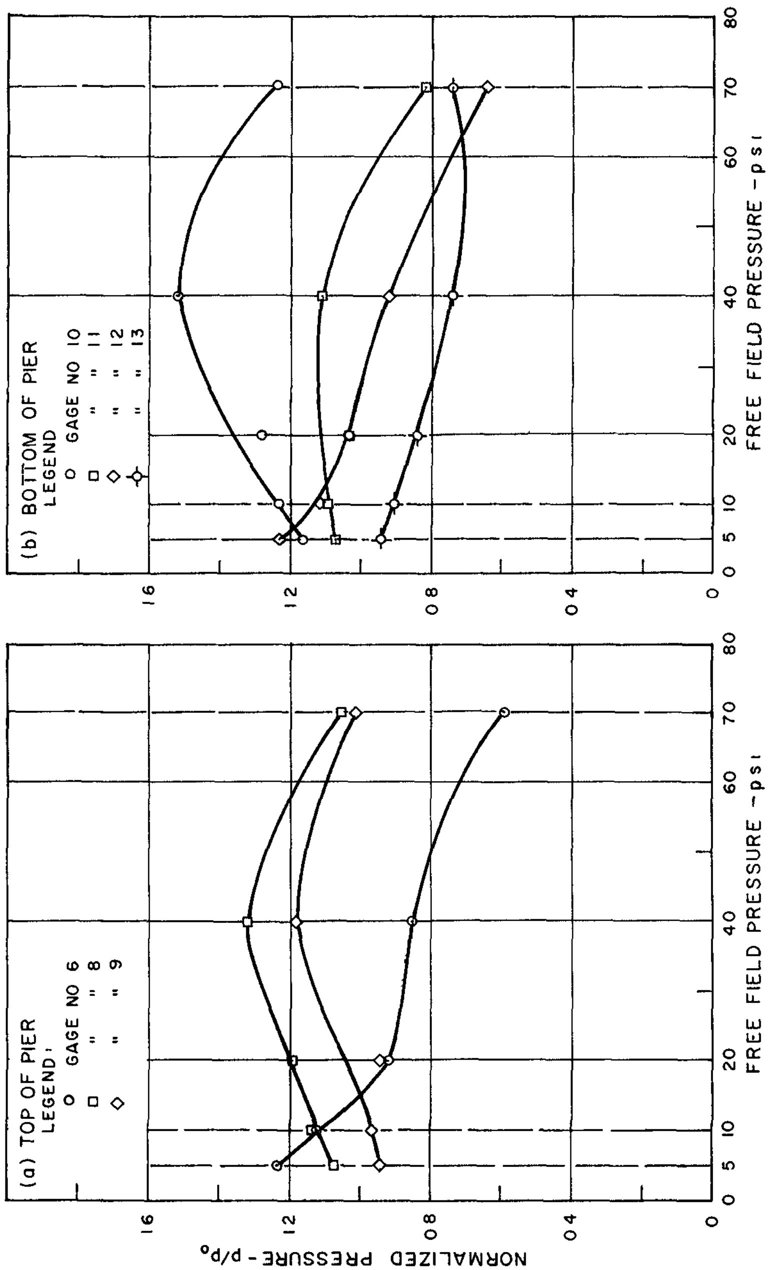

FIGURE 5 NORMALIZED PIER PRESSURE VARIATION WITH FREE FIELD PRESSURE

TEST SITUATION #1

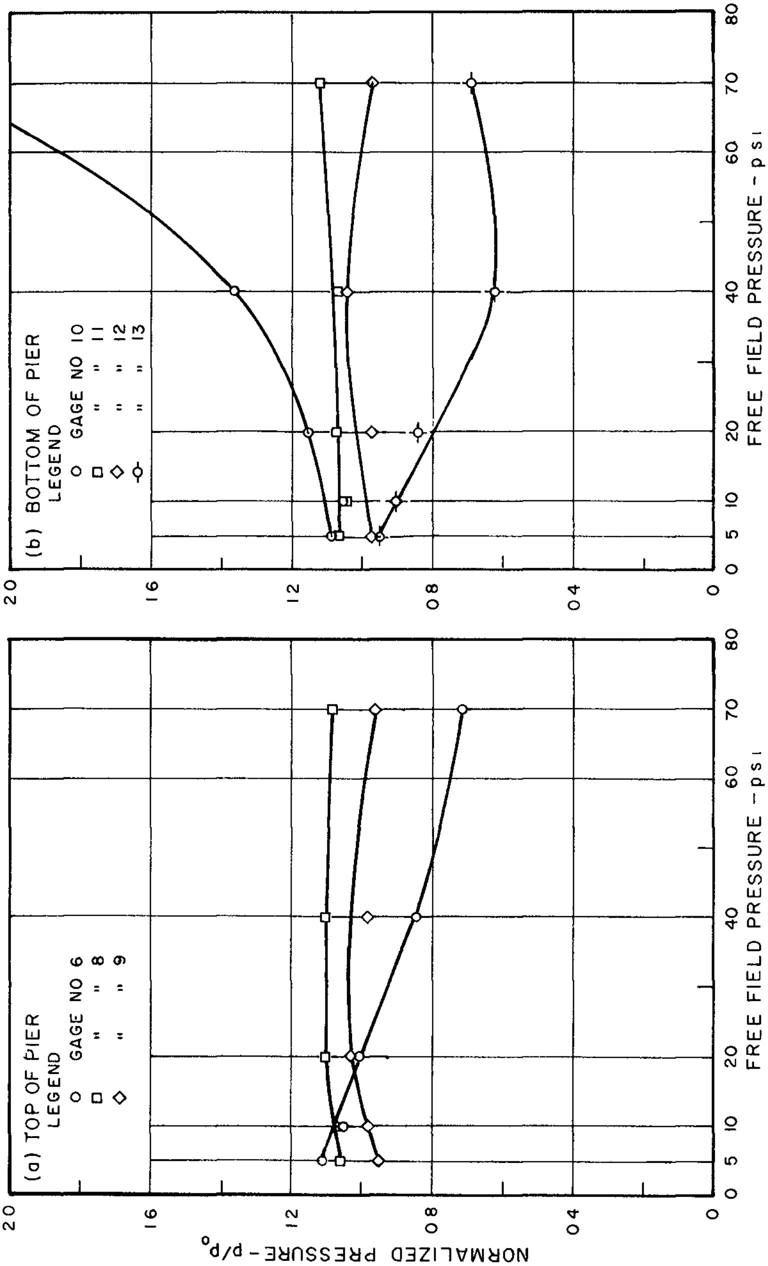

FIGURE 6 NORMALIZED PIER PRESSURE VARIATION WITH FREE FIELD PRESSURE
TEST SITUATION #2

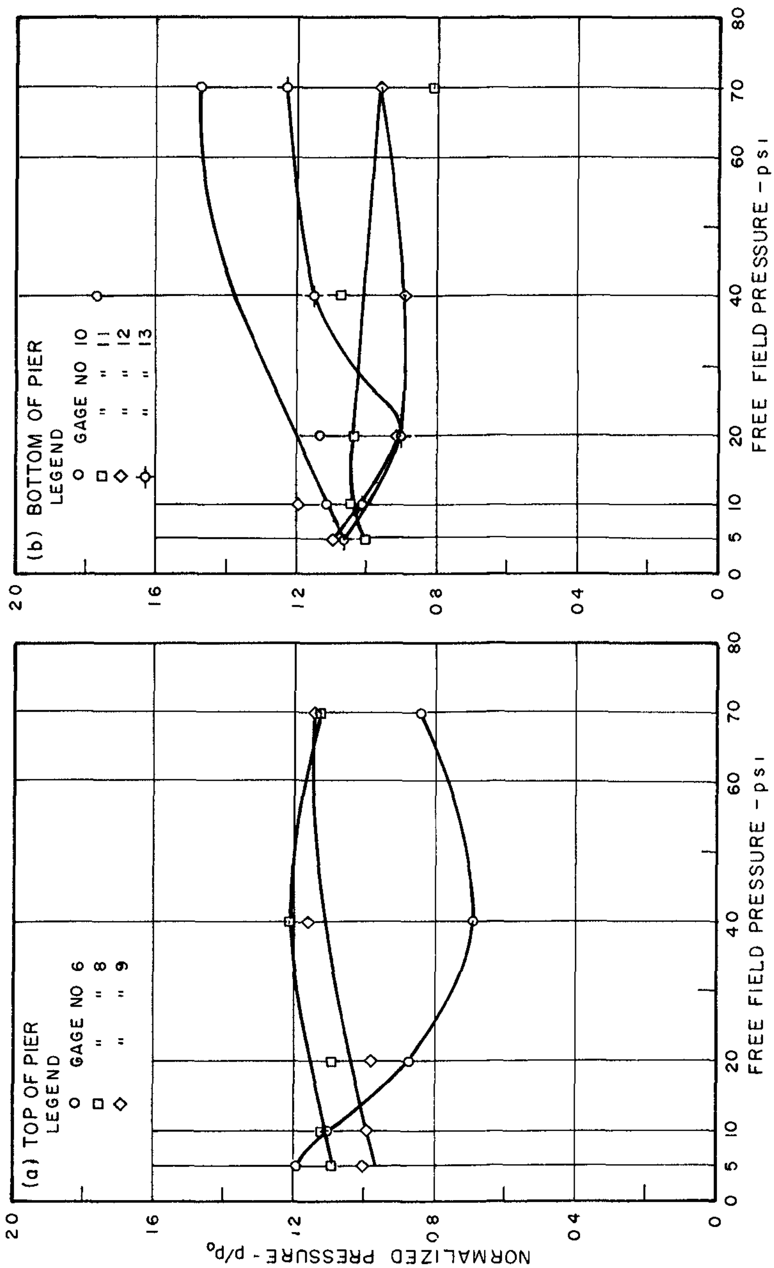

FIGURE 7 NORMALIZED PIER PRESSURE VARIATION WITH FREE FIELD PRESSURE

TEST SITUATION #3

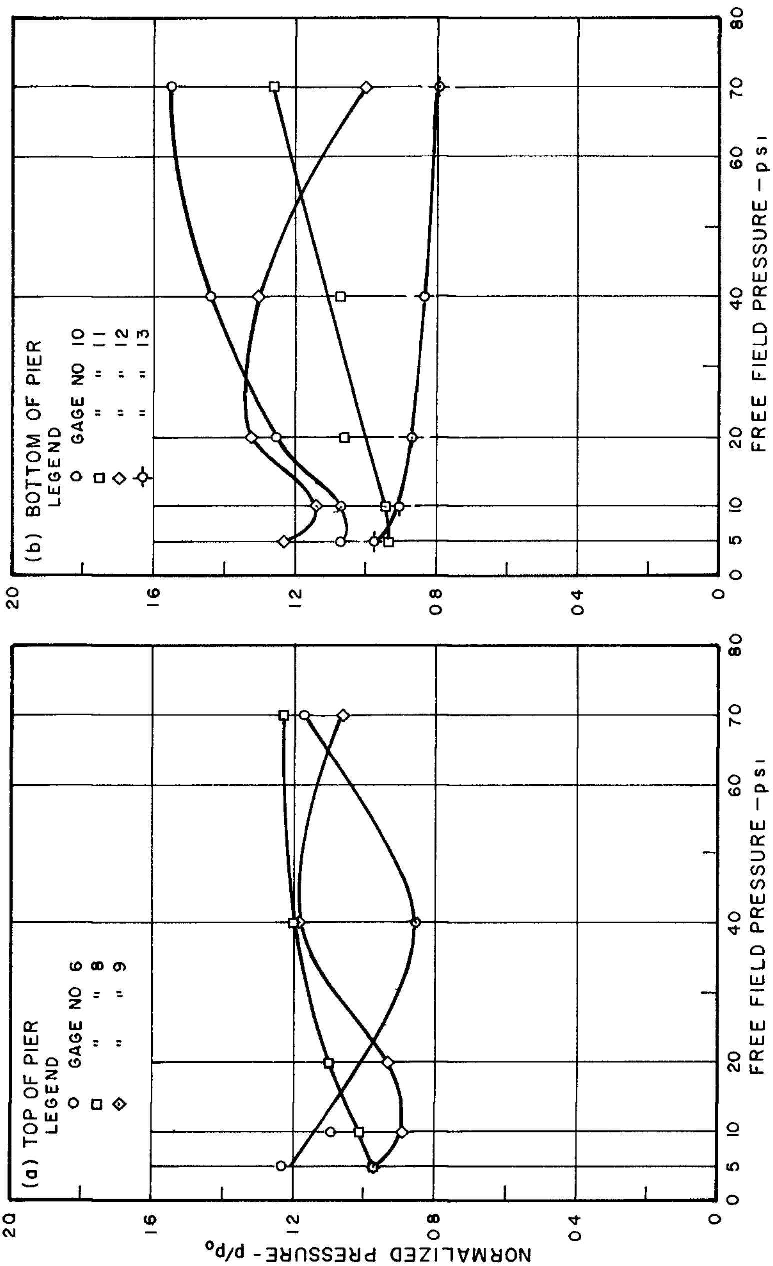

FIGURE 8 NORMALIZED PIER PRESSURE VARIATION WITH FREE FIELD PRESSURE

TEST SITUATION #4

pressure levels, but high shock pressures seem to result in appreciably higher loads on the deep water pier, possibly due to water wave impact. Fig. 8b shows the pressure on a pier in a regular reflection region. Here the loading on the front end of the pier is considerably lower at high shock loads than that experienced in the Mach reflection region (Fig. 6b). Otherwise the two regions do not give appreciably different results.

The theory discussed in a previous section of the paper has been applied to obtain graphically the solution for test situation No. 2 (pier on a dry beach), at free field overpressures of approximately 20 psi and 70 psi. These solutions are shown in Fig. 2a, b. For comparison the results are plotted in Fig. 9a, b, together with experimentally obtained values under similar conditions.

Fig. 9a, showing conditions of 20 psi, shows that the graphical solution results in maximum uplift pressure higher than maximum measured pressure. The distribution of uplift pressure over the length of the pier is quite different for the two cases. The experimental results show that the net uplift pressure decreases in the direction of the shock flow in contrast to the results predicted by the characteristic solution. Fig. 9b, which represents conditions at 70 psi, shows the same general features, although the very high uplift pressure measured at the front end of the pier exceeds the maximum uplift pressure obtained by the characteristic solution. These discrepancies between predicted and observed results indicate that the theoretical model should be modified to represent more closely actual conditions on the pier. Schlieren photographs would be of great value here and this technique should definitely be included in future test of this type. Until such results are available, the following factors can be listed as possible causes of discrepancy:

a. Since the pier model has a very low aspect ratio and a complicated geometry, the flow is three-dimensional. Thus the two-dimensional characteristic solution may not be appropriate to predict the actual flow properties.

b. All transducers except Nos. 6 and 10 are located in a region of shock expansion created by the supporting structure of the pier model which consists of cylindrical legs underneath and hexagonal units on top. The presence of these, which is not taken into account in the theoretical solution, definitely affects the flow field. It can be shown that their effect is to decrease the downstream pressure as observed in contrast with the theoretical results predicting increasing pressure when the cylindrical obstructions are neglected.

c. The shock front generated in the shock tube may not be plane as assumed.

Overpressure peaks on the pier caused by splashing water have been discussed in a previous section. It is possible that the water impact on the underside of the pier can result in much higher net uplift pressures than are caused by the passing shock wave. However, since relative wave arrival

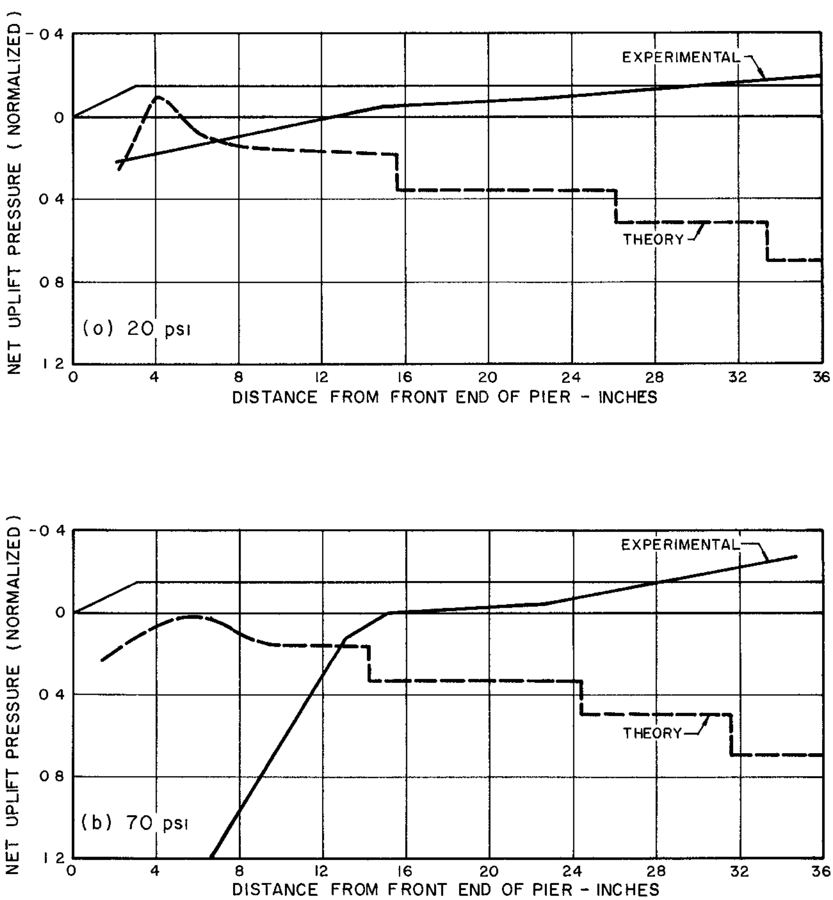

FIGURE 9 NET UPLIFT PRESSURE - THEORETICAL AND EXPERIMENTAL RESULTS FOR PIER ON DRY BEACH

times at each gage were not measured, the severity of the water impact effect cannot be evaluated. Future tests of this type should, therefore, be provided with equipment to measure these relative arrival times at each gage.

CONCLUSIONS

The findings of the study reported here may be summarized as follows:

1. Air shock loading on a pier on a dry sloping beach results in more severe uplift pressure than is experienced for the same configuration in the presence of water (test situation No. 1 vs. No. 2).

2. Air shock loading on a pier in water appears to be more severe in deep water than in shallow water (test situation No. 1 vs. No. 3). This is possibly due to water wave impact.

3. Air shock loading on a pier on a dry beach appears to be more severe when the pier is wholly located in the Mach reflection region than it is when the pier is partly in the regular reflection region (test situation No. 2 vs. No. 4).

4. It can be concluded from 1-3 above that test situation No. 2 - pier on a dry beach in a region of Mach reflection - will result in the most severe uplift pressures on the pier deck caused by the passing air blast wave.

5. Water waves caused by the air blast which splash against the underside of the pier may result in uplift pressures more severe than those caused by the air shock. Further tests are required to assess this effect.

6. Graphical solution for a pier in a region of Mach reflections (test situation No. 2), based on Whitham's diffraction theory, results in conservative estimates of the net uplift pressure at low incident pressures, but appears to underestimate this effect at high pressures. Further studies are required to make the theoretical model more realistic as well as to extend the technique, so that it may be applied to a pier in a region of regular reflection.

ACKNOWLEDGMENTS

The authors wish to express their gratitude to Mr. J. T. O'Brien of the Naval Civil Engineering Laboratory, Port Hueneme, California, for the many useful discussions throughout the course of this study. This investigation was supported by the U.S. Naval Civil Engineering Laboratory under Contract No. N62399-67-C-0049, and was sponsored by the Defense Atomic Support Agency, Washington, D. C. 20305.

REFERENCES

1. Glasstone, S., "The Effects of Nuclear Weapons," United States Atomic Energy Commission, April 1962.

2. Whitham, G. B., "On the Propagation of Shock Waves Through Regions of Non-Uniform Area of Flow," J. Fluid Mech., Vol. 4, pp. 337-360, 1958.

3. Whitham, G. B., "A New Approach to Problems of Shock Dynamics, Part I, Two-Dimensional Problems," J. Fluid Mech., Vol. 2, pp. 145-171, 1957.

4. Pack, D. C., "The Reflexion and Diffraction of Shock Waves," J. Fluid Mech., Vol. 18, pp. 549-576, 1964.

5. Lick, W., "The Shock-Expansion Method and Whitham's Rule," J. Fluid Mech., Vol. 25, pp. 179-184, 1966.

6. Chisnell, R. F., "A Note on Whitham's Rule," J. Fluid Mech., Vol. 22, pp. 103-104, 1965.

7. Miles, J. W., "A Note on Shock-Shock Diffraction," J. Fluid Mech., Vol. 22, pp. 95-102, 1965.

8. Bryson, A. E., Gross, R. W. F., "Diffraction of Strong Shocks by Cones, Cylinders, and Spheres," J. Fluid Mech., Vol. 10, pp. 1-16, 1961.

9. Holt, R. E. and Crist, R. A., "Calibration of a Six-Foot and a Two-Foot Diameter Shock Tube," AFSWC-TDR-63-5, Project No. 1080, Task No. 108005, Air Force Shock Tube Facility, Albuquerque, New Mexico, April, 1963.